ACS APPLIED MATERIALS & INTERFACES

Research Article

Cite This: ACS Appl. Mater. Interfaces 2018, 10, 28428−28439

www.acsami.org

Macromolecular Microencapsulation Using Pine Pollen: Loading Optimization and Controlled Release with Natural Materials

Arun K. Prabhakar,[†,‡,∥] Michael G. Potroz,[†,‡,∥] Ee-Lin Tan,[†,‡] Haram Jung,[†,‡] Jae Hyeon Park,[†,‡] and Nam-Joon Cho*[,†,‡,§]

[†]School of Materials Science and Engineering, Nanyang Technological University, 50 Nanyang Avenue, 639798, Singapore

[‡]Centre for Biomimetic Sensor Science, Nanyang Technological University, 50 Nanyang Drive, 637553, Singapore

[§]School of Chemical and Biomedical Engineering, Nanyang Technological University, 62 Nanyang Drive, 637459, Singapore

Supporting Information

ABSTRACT: Pine pollen offers an all-natural multicavity structure with dual hollow air sacs, providing ample cargo capacity available for compound loading. However, the pollen exhibits reduced permeability because of the presence of a thin natural water-proofing layer of lipidic compounds. Herein, we explore the potential for compound loading within pine pollen and the potential for developing all-natural formulations for targeted delivery to the intestinal tract. Removal of the surface-adhered lipidic compounds is shown to improve surface wetting, expose nanochannel structures in the outer pollen shell and enhance water uptake throughout the whole pollen structure. Optimization of loading parameters enabled effective compound loading within the outer pollen shell sexine structure, with bovine serum albumin (BSA) serving as a representative protein. All-natural oral delivery formulations for targeted intestinal delivery are developed based on tableting of BSA-loaded defatted pine pollen, with the incorporation of xanthan gum as a natural binder, or ionotropically cross-linked sodium alginate as an enteric coating. Looking forward, the large cargo capacity, ease of compound loading, competitive cost, abundant availability, and extensive historical usage as food and medicine make pine pollen an attractive microencapsulant for a wide range of potential applications.

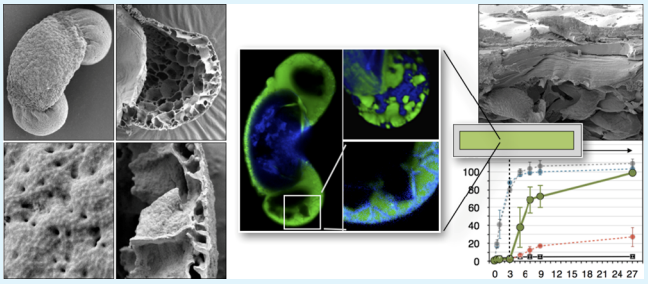

KEYWORDS: *pine pollen, microencapsulation, hollow microcapsules, targeted delivery, controlled release*

1. INTRODUCTION

Identifying novel natural materials for use in microencapsulation is of significant interest to a wide range of industries.[1−7] Pollen is a key example of nature's own evolutionary microencapsulation solution for the protection of sensitive genetic material crucial for reproductive success.[8,9] In general, pollen presents a wide range of properties desired of an ideal microencapsulant, such as, monodispersity, morphological stability, physicochemical resilience, and biocompatibility.[10−12] Most existing attempts to utilize pollen as a microencapsulant have involved the extraction of pollen sporoderm hollow shells through the use of various chemical extraction processes.[13−18] Sporoderm microcapsules (SDMCs) have been shown to provide a range of appealing properties, such as taste masking,[19] antioxidant protection,[20] UV protection,[21] immunomodulatory properties,[22] and ease of compound loading.[23] However, a primary limitation of SDMCs is that they require additional regulatory approval before being utilized for oral delivery applications in food and medicine, whereas natural pollens have a long history of use as food and medicine,[24−26] with natural pollen considered to be a regulation-free food ingredient in most parts of the world.[27,28] With the growing interest in utilizing pollen capsules as a microencapsulant, along with the inherent health benefits and the intriguing triple cavity structure of pine pollen, there is an opportunity to explore the challenges and potential solutions of using naturally porous saccate pollen, such as pine, as a microencapsulant.

Pine pollen possesses a triple cavity structure well suited to being used for microencapsulation, with two hollow air sac (bisaccate)[29,30] cavities providing ample space for compound loading.[31] Understanding and tuning the properties of the dual air sac pine pollen are crucial for successful compound loading within the air sac hollow cavities (Figure 1a). Studies have shown that the outer sporopollenin sexine shell of pine pollen air sacs is porous and permeable; however, these studies utilized air sacs extracted with extensive harsh chemical processing to isolate the shell material (sporopollenin) only.[32,33] Although the air sac structure is porous, studies with natural pine pollens (NPPs) have shown that a waterproofing layer of lipidic compounds reduces permeability and inhibits water uptake (Figure 1b).[34,35] The removal of the

Received: June 15, 2018
Accepted: July 26, 2018
Published: July 26, 2018

DOI: 10.1021/acsami.8b09952
ACS Appl. Mater. Interfaces 2018, 10, 28428−28439

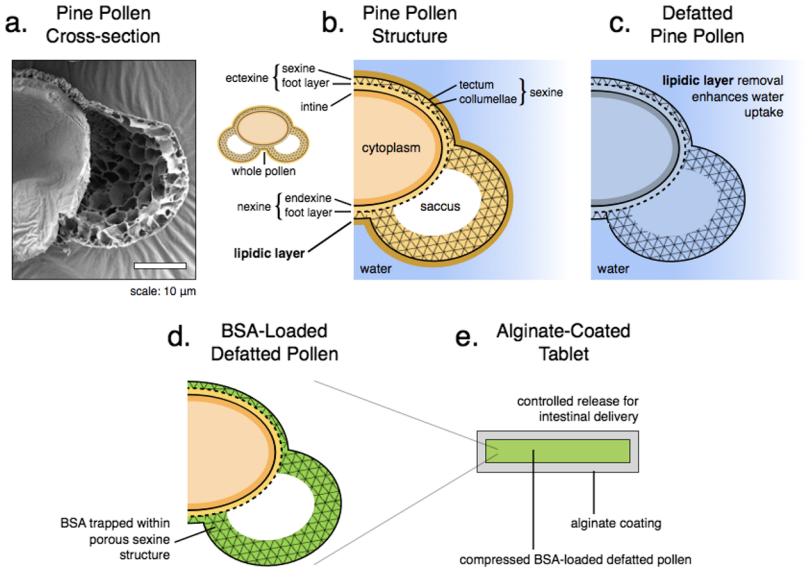

Figure 1. Schematic diagram showing the development of NPP multiparticulate tablets for intestinal protein delivery: (a) scanning electron micrograph of pine pollen capsule cross section, with emphasis on a single porous air sac (saccus) structure; (b) schematic representation of NPP structure, emphasizing resilience to water absorption; (c) defatting of pine pollen removes the external lipidic layer and enhances pollen water uptake; (d) BSA becomes trapped in the defatted pine pollen porous sexine structure; and (e) alginate-coated multiparticulate pine pollen tablet provides controlled release suitable for intestinal delivery of proteins.

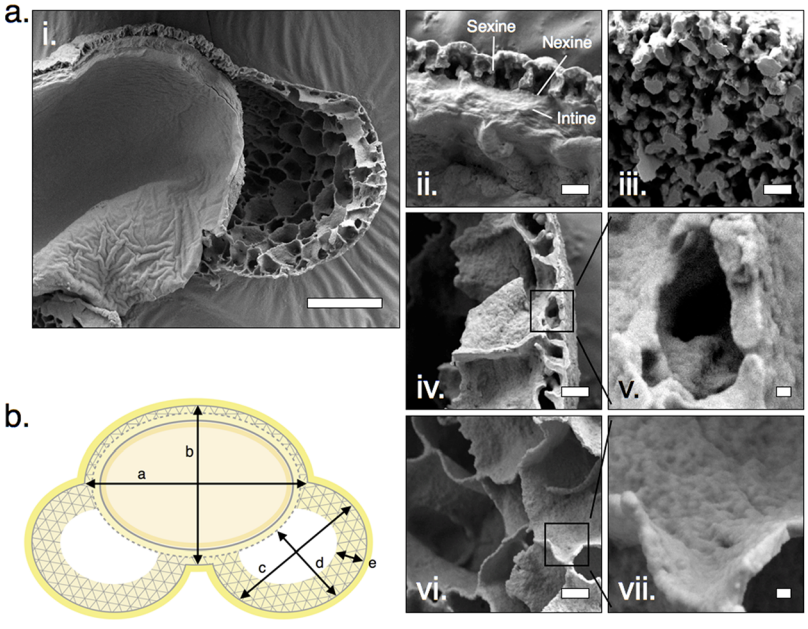

Dimensions (μm)	
a	43.5 ± 2.4
b	29.0 ± 3.3
c	25.4 ± 1.0
d	17.0 ± 1.9
e	3.5 ± 1.3

Region	Volume ($\times 10^3$ μm^3)	Proportion (%)
Central cavity	19.1 ± 5.4	58.2 ± 16.5
Sacci (Sacci Sexine)	11.5 ± 2.2 (6.7 ± 3.7)	37.5 ± 7.1 (21.8 ± 11.9)
Total	30.6 ± 7.6	100.0 ± 24.8

Figure 2. Pine pollen micro-/nanostructure and cargo capacity: (a) scanning electron micrograph of (i) pine pollen cross section, with close-up images of (ii) sexine, nexine, and intine structure around the central cavity, (iii) underside of the sexine structure with the nexine removed, (iv) cross section of the sexine structure around the saccus, (v) cross section of a single sexine cavity with external wall pore, (vi) internal sexine structure, and (vii) sexine wall; (b) schematic diagram and tables defining key pine pollen dimensions used for calculating volumes and volume proportions of particle, central cavity, sacci, and sacci sexine. Scale bars: (i) = 10 μm; (ii–iv,vi) = 1 μm; and (v,vii) = 100 nm.

DOI: 10.1021/acsami.8b09952
ACS Appl. Mater. Interfaces 2018, 10, 28428–28439

lipidic compound waterproofing layer from pine pollens with various organic solvents has been shown to facilitate water uptake[36] and may further facilitate compound loading within pine pollen sacci.

Herein, we explored the utilization of pine pollen (*Pinus massoniana*) for compound loading and developed a multiparticulate tableted oral delivery formulation, exhibiting controlled release suitable for intestinal delivery. Washing and defatting of raw pollen were conducted to obtain monodisperse NPP, single-defatted pine pollen (SDPP), and double-defatted pine pollen (DDPP). Fundamental morphological and compositional particle properties were analyzed to determine the influence of defatting. Changes in surface porosity and wetting due to defatting were examined and related to particle water absorption dynamics (Figure 1c). Compound loading optimization was conducted with bovine serum albumin (BSA), as a representative protein, to determine the vacuum-assisted loading and washing parameters required for optimal compound loading. Compound loading distribution studies were performed to gain insight into compound loading dynamics and further elucidated compound loading potentials (Figure 1d). Compound release studies were conducted with tableted BSA-loaded DDPP formulations, comprising either xanthan gum as a binder or ionotropically cross-linked sodium alginate as an enteric coating. Finally, tablets exhibiting ideal compound release profiles were examined to elucidate the morphological properties of multiparticulate tablets (Figure 1e).

2. EXPERIMENTAL SECTION

2.1. Materials. BSA, fluorescein isothiocyanate (FITC)-conjugated BSA, xanthan gun, sodium alginate, calcium chloride, and diethyl ether were purchased from Sigma-Aldrich (Singapore). Raw pine pollen (*P. massoniana*) was purchased from Xi'an Yuensun Biological Technology Company Limited (China). Milli-Q water was used in all experiments. A stainless steel pellet press die (13 mm) was purchased from Specac (Kent, UK).

2.2. Preparation of Pine Pollen. NPP (30 g) was suspended in deionized (DI) water (1 L) and vacuum-filtered a total of four times to remove dust and other smaller plant debris, followed by an additional filtration step with a nylon mesh (100 μm) to separate out any large debris, while allowing the smaller pollen particles to pass through. The pollen was then freeze-dried to obtain clean dry NPP powder. NPP (30 g) was treated with diethyl ether (300 mL) for 3.5 h with stirring (200 rpm), after which the solution was vacuum-filtered and vacuum-oven-dried until stable weight (100 mbar, 40 °C, 30 min) to remove any traces of ether. A single defatting step produced single-defatted pollen. SDPP (10 g) was treated with diethyl ether (100 mL) with stirring (200 rpm) for 3.5 h, after which the pollen was vacuum-filtered and dried (100 mbar, 40 °C, 30 min) to obtain dry double-defatted pollen.

2.3. Pollen Particle Characterization. *2.3.1. Surface Morphology Evaluation.* Scanning electron microscopy (SEM) imaging was performed using JSM 5410 (JEOL, Tokyo, Japan). Samples were sputter-coated to obtain a 10 nm thick gold film using a JFC-1600 instrument (JEOL, Tokyo, Japan) (20 mA, 60 s). Images were captured at an accelerating voltage of 5 kV at different magnifications. For particle cross sections, particles were adhered to the carbon tape and then submerged in liquid nitrogen for ~20 s, followed by cutting across the adhered pollen multiple times with a scalpel blade. Cross-sectioned particles were identified by examining cut marks during imaging.

2.3.2. Volumetric Calculations. On the basis of models presented from previous studies,[31,37] the central cavity volume was calculated based on an ellipsoid and the air sac volumes were calculated as half of an ellipsoid each. Central cavity ellipsoid radii: $r_1 = a/2$, $r_2 = b/2$, and $r_3 = b/2$. Air sac ellipsoid radii: $r_1 = d$, $r_2 = c/2$, and $r_3 = c/2$. Dimensions (a–e), defined in Figure 2b.

2.3.3. Micromeritic Properties. Dynamic imaging particle analysis (DIPA) was performed using a FlowCam benchtop system (FlowCam VS, Fluid Imaging Technologies, Maine, USA) equipped with a 200 μm wide flow cell (FC-200) and 20× magnification lens (Olympus, Japan). NPP and defatted pine pollen suspensions (2 mg/mL) were sonicated in a water bath (10 min) and filtered through 100 μm filter mesh prior to analysis. The samples were then manually added into the flow cell via a pump-controlled syringe and analyzed at a fixed flow rate (0.1 mL/min). Particle morphology analysis was performed on well-focused particles only (n = 3000), and data presented are representative of three independent data sets.

2.3.4. Elemental CHN Analysis. A VarioEL III elemental analyzer (Elementar, Hanau, Germany) provided CHN analysis to determine the amount of nitrogen and estimate the amount of protein in the pollen. All samples were dried under vacuum (60 °C, 1 h, 1 mbar) before being combusted in excess oxygen at high temperature to release compositional carbon, hydrogen, and nitrogen. All measurements were conducted in triplicate.

2.4. Pine Pollen Wetting and Hydration. *2.4.1. Contact Angle.* A single layer of carbon tape was stuck onto a glass slide after which the dry pollen powder (NPP, SDPP, and DDPP) was dropped onto the surface to form a thin layer. DI water (2 μL) was dropped onto the layer, and the contact angle was measured until the drop stabilized (10 s).

2.4.2. Porosity Analysis (N_2 Adsorption–Desorption). Pollen (300 mg) was added into glass tubes and degassed (2 h, 130 °C) to remove any bound molecules. Liquid nitrogen was filled into Dewar flasks, and then the tubes were fixed onto the apparatus (ASAP TriStar II 3020), and the setup was left overnight for a complete adsorption–desorption cycle. Brunauer–Emmett–Teller (BET) theory was used to calculate the specific surface area of the particles assuming multilayer adsorption, whereas the Barrett–Joyner–Halenda (BJH) method was used to determine the pore size distribution.

2.4.3. Water Permeability Testing. Passive water-loaded pine pollen was obtained by combining NPP, SDPP, and DDPP (10 mg each) with DI water (1 mL) to ensure complete wetting, whereupon the samples were mixed on an orbital shaker (500 rpm) and then observed under an optical microscope at fixed time points (5, 15, 30, 60, 120 min, and 24 h). Vacuum water-loaded pine pollen was obtained by combining NPP, SDPP, and DDPP (10 mg each) with DI water (1 mL) to ensure complete wetting, whereupon the samples were subject to vacuum (0.01 mbar, 5 min) and then observed under an optical microscope. The particle fraction of completely water-filled pollen was quantified (%) at each time point (for both passive and vacuum-assisted methods) by analysis of three optical microscopy images with a minimum of 30 pollen particles per image.

2.5. Compound Encapsulation. *2.5.1. BSA Encapsulation.* Passive loading of BSA was achieved by combining NPP (50 mg) with a BSA solution (50 mg/mL, 1 mL) and mixing on a shaker (500 rpm, 1 h). Vacuum loading of BSA was achieved by combining NPP (50 mg) with a BSA solution (50 mg/mL, 1 mL) and vortexing (30 s) to ensure uniform mixing, after which it was subject to vacuum loading (0.01, 1, 100, and 1000 mbar) for varying time points (5, 15, 30, and 60 min) to determine minimum requirements for optimum loading. After optimizing vacuum duration and vacuum pressure, BSA loading solution concentration was varied (12.5 and 25 mg/mL) to explore the influence of BSA concentration on BSA loading. After optimizing vacuum duration, vacuum pressure, and BSA concentration for NPP, both SDPP and DDPP were loaded under the same optimal loading conditions to explore the influence of defatting on the BSA loading of pine pollen. Finally, for DDPP, loading solution volumes were varied (0.25, 0.33, 0.5, 1.0, 2.0, 3.0, and 4.0 mL) with a fixed pollen mass (50 mg), to explore the influence of BSA loading solution volume on BSA loading. All formulations were washed with water and freeze-dried and stored in a dry cabinet until analysis.

2.5.2. BSA-Loaded Pollen Washing. For BSA-loaded NPP, DI water (1 mL) was added to BSA-loaded pollen (25 mg) and centrifuged (13 500 rcf, 3 min) before discarding the supernatant; this

DOI: 10.1021/acsami.8b09952
ACS Appl. Mater. Interfaces 2018, 10, 28428–28439

washing step was repeated for a total of two times, and the washed BSA-loaded pollen was then freeze-dried. BSA-loaded defatted pine pollen washing utilized a reduced centrifugation duration (SDPP—2 min, DDPP—1 min). All dried samples were inspected, and any excess large agglomerates of BSA were removed by spatula.

2.5.3. Loading Efficiency. BSA-loaded pollen (10 mg) was ground using a mortar and pestle (5 min), mixed with phosphate-buffered saline (2 mL), vortexed (5 min), and centrifuged (17 000 rcf, 5 min). The supernatant was filtered using a 0.45 μm PES syringe filter (Agilent, CA, USA). The absorbance values were measured at 280 nm (BOECO-S220, Germany) using unloaded pollen as a blank, and the amount of BSA present in the BSA-loaded pollen was calculated using a BSA standard curve. The loading efficiency of BSA in the BSA-loaded pollen was calculated with the following formula.

$$\text{BSA loading efficiency (\%)} = \frac{\text{BSA (mg)}}{\text{BSA-loaded pollen (mg)}} \times 100\%$$

To estimate the theoretical maximum loading efficiency for when the volumetric BSA loading is 100 vol %, a multiplication factor was determined based on achieved volumetric loading (58 vol % × 1.72 = 100 vol %). A BSA/pollen weight loading ratio is calculated from the achieved loading efficiency (10.6% loading efficiency = 0.12:1 BSA/pollen weight loading ratio). The weight proportion of BSA is increased by the multiplication factor (0.12 × 1.72 = 0.21). The theoretical maximum loading efficiency is determined from the maximum BSA/pollen weight loading proportion (0.21:1 = 17.4% loading efficiency).

2.5.4. Loading Distribution. Pine pollen samples were mounted on slides with VECTASHIELD and scanned via confocal laser scanning microscopy (CLSM, Carl Zeiss LSM700, Germany). Laser excitation lines were set to 405, 488, and 561 nm at a scan speed of 67 s per phase. Images were collected with differential interference contrast at 405 nm (6.5%), 488 nm (6%), and 561 nm (6%) using enhanced-contrast Plan-Neofluar 20×, 40×, and 63× oil objective M27 lenses. The fluorescence emission was collected in photomultiplier tubes equipped with different filters (416−477, 498−5, and 572−620 nm) and analyzed by using ZEN software. Fluorescence intensities of samples were compared utilizing ImageJ. Green channels of images were used for intensity quantification of FITC-BSA loading. The total intensity of each image was quantified, and this value was divided by the number of particles per image to obtain the average intensity per particle. Analysis was repeated for three images per sample to obtain triplicate values for average intensity per particle.

2.6. Tableting and Controlled Release. *2.6.1. Tablet Formation.* Tablets were formed with only BSA-loaded DDPP, with the addition of xanthan gum as a binder, or with an additional calcium alginate coating. All tablets were formed using a hydraulic press (5 t, 20 s, 132.75 mm^2 cross-sectional area, 370 MPa compression pressure).[38] Pure pollen tablets for use as controls were made from 150 mg of DDPP, whereas BSA-encapsulated pollen tablets were made out of 163 mg (150 mg DDPP + 13 mg of encapsulated BSA) BSA-loaded DDPP. Tablets with an additional xanthan gum binder were prepared with BSA-loaded DDPP (163 mg) plus varying proportions of powdered dry xanthan gum (1, 2.5, 5, 10, 20, and 30 w/w %), and xanthan gum no-pollen control tablets were prepared comprising BSA (13 mg) and xanthan gum (150 mg). Tablets for calcium alginate coating were prepared with BSA-loaded DDPP (163 mg) and then coated. Alginate coating involved dipping tablets in sodium alginate solution (2 w/v % in DI water, 5 s) followed by dipping in calcium chloride solution (4 w/v % in water, 10 s) as a single coating cycle, the dipping in sodium alginate solution and calcium chloride solution was then repeated for a total of two times each. Alginate-coated tablets were air-dried in a fume hood (12 h) followed by vacuum drying until stable weight (200 mbar, 24 h). Sodium alginate no-pollen control tablets were prepared comprising BSA (13 mg) and sodium alginate (150 mg) with a double coating cycle as described above.

2.6.2. Compound Release. Powdered formulations of BSA-loaded DDPP powder (with 2 mg BSA equivalent) were dissolved in simulated gastric fluid (SGF) (4 mL) and simulated intestinal fluid (SIF) (4 mL) separately, with release solution (1 mL) being removed at fixed time points and replaced with fresh solution (1 mL). The BSA content of the release solution was determined by measuring absorbance values at 280 nm (BOECO-S220, Germany). A blank formulation (unloaded pollen) was also tested in the same way as to negate the possible influence of natural pollen protein release. The difference in the absorbance values of the BSA-loaded sample and the blank gave the BSA mass released. Tableted formulations were first added to SGF (20 mL) for 3 h, after which the release medium was replaced with SIF for 24 h. The release solution (1 mL) was removed at fixed time points and replaced with fresh solution (1 mL). The BSA content of the release solution was determined by measuring absorbance values at 280 nm (BOECO-S220, Germany) and compared with a blank to determine BSA release.

2.7. Statistical Analysis. Where there is no other indication, all of the data were collected and are presented in triplicate (n = 3). Significance testing was performed using two-tailed t-tests, and $P < 0.05$ was considered as statistically significant.

3. RESULTS AND DISCUSSION

To determine the overall potential of compound loading within pine pollen, it is important to assess the structure and volume of the hollow regions within the pollen. Morphological observations of pine pollen cross sections indicate that the air sacs may be categorized into two distinct regions, the outer porous sexine structure and the inner hollow cavity region (Figure 2a; Figure S1, Supporting Information). It should be noted that the sexine region around the central cavity does comprise a thin porous layer; however, volumetric estimations of only the air sacs may be adequate for determining overall loading potential. The outer porous sexine structure comprises micron-sized cavities separated by smooth cavity walls (Figure 2a). Pollen morphological analysis resulted in the determination that pine pollen sacci constitute over a third of the total volume of a pollen particle, with the sacci porous sexine structure constituting approximately a fifth of the total pollen volume (Figure 2b). A potential volumetric cargo capacity of 37.5 ± 7.1% strongly supports the potential use of pine pollen for microencapsulation applications.

3.1. Pollen Wetting and Hydration. Preprocessing and defatting of raw pine pollen were undertaken for the removal of contaminants and surface-adhered lipidic compounds and resulted in substantial reductions in final pollen yields. Initial preprocessing steps of water washing, filtration, and freeze-drying removed contaminants and produced a more homogeneous dry pollen sample with a yield of 77.6 ± 1.1%. Pollen defatting further decreased pollen yields, with a single defatting step and double defatting step producing final yields of 74.3 ± 3.1 and 62.9 ± 5.5%, respectively. The reduction of pollen yields from defatting highlights that NPP possesses a large portion of surface-adhered lipidic compounds.

3.1.1. Morphological and Bulk Analysis. DIPA indicated that pollen defatting had negligible effect on pollen morphology (Figure S2, Supporting Information). The average particle diameter and particle size distribution of NPP, SDPP, and DDPP were similar, at 58.57 ± 1.16, 58.21 ± 0.62, and 62.19 ± 1.93 μm, respectively (Figure S2d, Supporting Information). With regards to shape, all of NPP, SDPP, and DDPP exhibited similar morphological features such as aspect ratio and circularity (Figure S2e,f, Supporting Information). These parameters show that pine pollen is physically intact after defatting with no significant collapsing or breaking occurring, thus confirming the mild nature of the defatting process.

DOI: 10.1021/acsami.8b09952
ACS Appl. Mater. Interfaces 2018, 10, 28428−28439

Elemental analysis indicated that pollen defatting caused no removal of the pine pollen's proteinaceous cytoplasmic contents. The percentage of nitrogen content of plant-based materials can be used to estimate percent protein content by application of a multiplication factor of 6.25.[39] The percent nitrogen content for NPP, SDPP, and DDPP was found to be 1.6 ± 0.0, 1.6 ± 0.1, and 1.6 ± 0.1%, respectively (Table S1, Supporting Information). The stability of percent nitrogen suggests that the defatting process has no significant effect on cytoplasmic constituents of the pollen.

3.1.2. Surface and Porosity Analysis. Contact angle measurements indicated that pine pollen becomes more hydrophilic with increased defatting. Microparticle coatings of NPP exhibit a contact angle of 83.3 ± 0.4°, with SDPP and DDPP exhibiting contact angles of 50.7 ± 1.9 and 17.3 ± 9.6°, respectively (Table 1). The increase in hydrophilicity observed with defatting may be attributed to the removal of surface-adhered lipidic compounds that are inherently hydrophobic.

Table 1. Contact Angle, Cumulative Pore Surface Area and Volume, and Average Pore Width of NPP, SDPP, and DDPP[a]

	NPP	SDPP	DDPP
contact angle (degrees)	83.3 ± 0.4	50.7 ± 1.9	17.3 ± 9.6
BET surface area (m^2/g)	0.53 ± 0.08	1.36 ± 0.15	1.37 ± 0.22
cumulative surface area of pores (m^2/g)	0.23 ± 0.05	0.46 ± 0.05	0.51 ± 0.08
cumulative volume of pores ($\times 10^9 m^3/g$)	3.91 ± 0.21	5.16 ± 0.51	5.44 ± 0.70
average pore width (nm)	29.7 ± 4.4	16.0 ± 0.8	16.5 ± 0.8

[a]NPP—natural pine pollen, SDPP—single-defatted pine pollen, DDPP—double-defatted pine pollen.

Nitrogen adsorption−desorption isotherm analysis showed that pollen defatting increased specific surface area, surface area of pores, volume of pores, and decreased average pore width. The N_2 sorption isotherms are characteristic of type IV isotherms typically associated with mesoporous materials.[40] The NPP exhibited a BET theory surface area of 0.53 ± 0.08 m^2/g and SDPP and DDPP with 1.36 ± 0.15 and 1.37 ± 0.22 m^2/g, respectively (Table 1). The increase in specific surface area with defatting may be attributed to exposing additional nanopores during the defatting process. The cumulative surface area of pores increased with the degree of defatting, with NPP exhibiting 0.23 ± 0.05 m^2/g and SDPP and DDPP with 0.46 ± 0.05 and 0.51 ± 0.08 m^2/g, respectively. Correspondingly, the cumulative volume of pores also increased with the degree of defatting, with NPP exhibiting 3.91 ± 0.21 × 10^9 m^3/g, and SDPP and DDPP with 5.16 ± 0.51 × 10^9 and 5.44 ± 0.70 × 10^9 m^3/g, respectively. The increase in cumulative surface area and cumulative volume of pores indicates that defatting increases the quantity of pores. The BET average pore size of defatted pollen is smaller than that of natural pollen, with NPP exhibiting an average pore width of 29.7 ± 4.4 nm, and SDPP and DDPP with 16.0 ± 0.8 and 16.5 ± 0.8 nm, respectively. The BJH desorption pore diameter distribution indicates that NPP, SDPP, and DDPP all exhibit a peak pore diameter of ∼45 nm (Figure 3a), with SDPP and DDPP exhibiting a distribution of pores below 4.6 nm diameter as well. The presence of nanopores below 4.6 nm diameter may be attributed to the removal of surface-adhered lipidic compounds from the multilevel helical sporopollenin subunits of the exine as defined in previously published studies.[41]

Morphological observations of the pollen surface, by SEM, before and after defatting, indicated that defatting effectively removes surface-adhered lipidic material and exposes a higher density of nanopores in the outer exine shell surrounding both the central cavity and the air sacs (Figure 3b). Exposed visible pore sizes are in the range of 30−100 nm, with the majority of nanopores being ∼50 nm. The exposure of numerous small pores may be expected to aid in enhanced and more rapid compound loading.

3.1.3. Membrane Permeability Analysis. Particle water uptake was explored by exposing natural and defatted pine pollen to both passive and vacuum-assisted loading methods. Passive and vacuum-assisted loading of water into natural and defatted pine pollen indicated that water filling rates increase with greater defatting, with DDPP exhibiting the fastest overall water uptake and greatest portion of loaded particles. Passive loading showed that NPP is poorly penetrated by water with only 7.2 ± 0.8% of the particles completely filled (becoming transparent) even after 24 h (Figure 3c,d; Figure S3, Supporting Information). Whereas, for passive loading, the proportion of full SDPP increases to 61.1 ± 12.0% within 60 min and remains stable to 24 h, and the proportion of full DDPP increases to 73.7 ± 2.8% within 30 min and remains stable to 24 h (Figure 3d; Figure S3, Supporting Information). Overall, these observations suggest that defatted pollen may facilitate the loading of hydrophilic molecules faster and more efficiently than natural pollen because of enhanced water flux.

Vacuum loading showed that air sac water filling could be enhanced for defatted pine pollen with the application of a vacuum for only 5 min, while providing no enhancement with NPP. Short-duration vacuum loading achieved 82.9 ± 14.3 and 94.3 ± 4.1% of full particles for SDPP and DDPP, respectively, with NPP exhibiting only 0.7 ± 0.9% of full particles (Figure 3d; Figure S3, Supporting Information). The increased proportion of filled air sacs and overall filling, observed with vacuum loading of defatted pollen, may be attributed to water being drawn into the air sac cavity because of air being forcefully extracted by a negative pressure differential resulting from the creation of an external low pressure region by the application of a vacuum.[38]

3.2. Compound Encapsulation. Optimization of BSA loading in natural pollen was explored with vacuum loading to gain insight into the ideal parameters and limits of compound loading in NPP. After significant parameter variation, it was determined that the application of a vacuum with a pressure of 1 mbar, for 5 min, with a BSA loading concentration of 50 mg/mL, could achieve a maximum BSA loading efficiency in NPP of 5.8 ± 0.7% (Figure 4).

3.2.1. Loading Method and Parameter Optimization. Vacuum loading was shown to produce greater loading efficiencies than passive loading. During the first step of vacuum-assisted BSA loading optimization, it was determined that vacuum pressures of 1 and 0.01 mbar produced maximum loading efficiencies which were statistically equivalent (p = 0.25). Overall, loading pressures of 1000, 100, 1, and 0.01 mbar produced loading efficiencies of 2.3 ± 0.4, 2.5 ± 0.5, 5.8 ± 0.7, and 6.5 ± 1.7%, respectively (Figure 4a). Vacuum loading at 0.01 mbar achieved ∼3 times greater loading than passively loaded samples (1000 mbar), which is in line with existing research with other pollen species and particles.[42,43]

DOI: 10.1021/acsami.8b09952
ACS Appl. Mater. Interfaces 2018, 10, 28428−28439

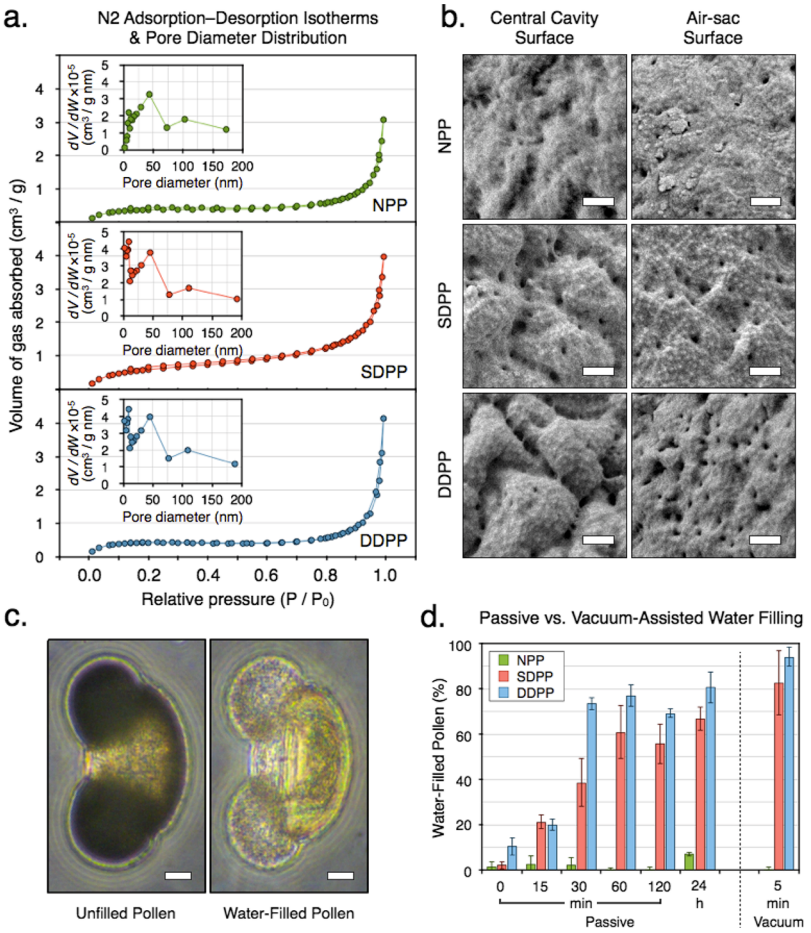

Figure 3. Surface properties and water uptake of natural and defatted pine pollen: (a) nitrogen adsorption−desorption isotherms with pore diameter distributions of NPP, SDPP, and DDPP; (b) scanning electron micrographs of central cavity and air sac surfaces of NPP, SDPP, and DDPP; (c) optical microscopy images of unfilled and water-filled NPP; and (d) proportion of pollen particles with water-filled air sacs with passive and vacuum-assisted loading. NPP: natural pine pollen, SDPP: single-defatted pine pollen, DDPP: double-defatted pine pollen. Scale bars: (b) = 500 nm, (c) = 10 μm.

During the second step of vacuum-assisted BSA loading optimization, it was determined that a vacuum application duration of 5 min was sufficient to achieve the maximum loading efficiency. Overall, vacuum application durations of 5, 15, 30, and 60 min produced loading efficiencies of 6.5 ± 1.7, 7.0 ± 0.8, 6.4 ± 0.9, and 6.5 ± 1.7%, respectively (Figure 4b). Statistical analysis of this data indicates that loading efficiencies for varying vacuum application durations are statistically equivalent (p = 0.95 for the time points 5 and 15 min). From observations during sample preparation, it appears that short vacuum application durations are adequate due to rapid evaporation of aqueous loading solutions under vacuum conditions.

During the third and final step of vacuum-assisted BSA loading optimization, it was determined that a BSA loading solution concentration of 50 mg/mL achieved the maximum loading efficiency. Overall, BSA loading solution concentrations of 12.5, 25, and 50 mg/mL produced loading efficiencies of 3.0 ± 0.3, 4.5 ± 1.1, and 6.5 ± 1.7%, respectively (Figure 4c). The data indicate that the amount of BSA in the BSA-loaded pine pollen is directly proportional to the amount of BSA in the BSA loading solution.

Comprehensive optimization of BSA loading parameters for vacuum-assisted loading of NPP highlighted the importance of high loading solution concentration and the application of an adequately low vacuum pressure and indicated that maximum loading may be achieved within a short duration of vacuum application. To allow for the potential of further system variation, the loading parameters used for the remainder of this study were determined to be the application of a vacuum with a pressure of 0.01 mbar, for 5 min, with a BSA loading concentration of 50 mg/mL.

3.2.2. Washing and Pollen Loading Optimization. The influence of the washing of BSA-loaded natural pollen was explored to optimize the washing conditions so as to achieve maximum loading efficiencies while ensuring adequate removal of surface-adhered BSA. On the basis of SEM analysis of BSA-loaded NPP particle cleanliness for zero, one, and two water washes, it was determined that two water washes (0.5 mL each) resulted in adequate removal of surface-adhered BSA (Figure 4d; Figure S4a, Supporting Information). Overall, zero, one, and two water washes of BSA-loaded NPP produced loading efficiencies of 28.4 ± 2.4, 13.8 ± 1.0, and 6.5 ± 1.7%, respectively (Figure 4e). However, application of the NPP two-wash protocol to BSA-loaded SDPP and DDPP resulted in lesser loading, with SDPP and DDPP producing loading efficiencies of 4.2 ± 2.2 and 2.9 ± 2.0%, respectively (Figure 4f). Because of defatted pollen exhibiting a more rapid uptake of water, further optimization of the washing protocol was undertaken with a reduction of washing cycles and

DOI: 10.1021/acsami.8b09952
ACS Appl. Mater. Interfaces 2018, 10, 28428−28439

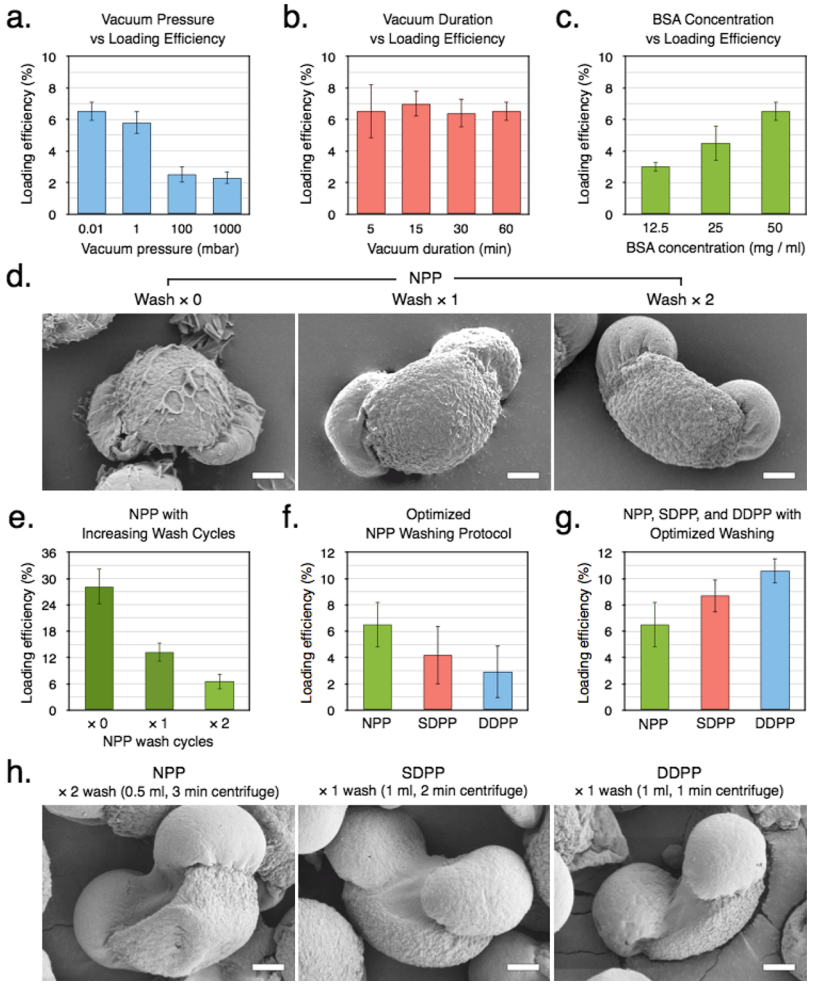

Figure 4. Loading parameter and washing optimization for BSA loading in natural and defatted pollen: (a) effect of vacuum pressure on BSA loading potential; (b) effect of vacuum duration on BSA loading potential; (c) effect of BSA loading solution concentration on BSA loading potential; (d) scanning electron micrographs of BSA-loaded NPP at each washing step; (e) loading efficiency of BSA-loaded NPP at each washing step; (f) loading efficiency of BSA-loaded NPP, SDPP, and DDPP with application of optimized NPP washing protocol; (g) loading efficiency of BSA-loaded NPP, SDPP, and DDPP with optimized washing protocols; and (h) scanning electron micrographs of BSA-loaded NPP, SDPP, and DDPP after application of optimized washing centrifugation duration. NPP: natural pine pollen, SDPP: single-defatted pine pollen, DDPP: double-defatted pine pollen. Scale bars: 10 μm.

centrifugation time. Centrifugation durations of 3 min (2 washes of 0.5 mL each), 2 min (1 wash of 1 mL), and 1 min (1 wash of 1 mL), for NPP, SDPP, and DDPP, respectively, were found to produce loading efficiencies of 6.5 ± 1.7, 8.7 ± 1.2, and 10.6 ± 0.9% (Figure 4g) and resulted in adequate removal of surface-adhered BSA (Figure 4h; Figure S4b, Supporting Information). Variations in loading and washing dynamics of natural and defatted pine pollen may be attributed to increases in porosity and water permeability with increased defatting.

On the basis of DDPP facilitating maximum loading, further variation of loading solution volumes indicated that the initial loading solution volume of 1 mL per 50 mg pollen (20 μL/mg) achieved an optimal loading efficiency of 10.6 ± 0.9%. By retaining a loading solution concentration of 50 mg/mL and reducing the amount of loading solution used, it was determined that volumes of 0.25, 0.33, and 0.5 mL produced maximum loading efficiencies of 4.5 ± 0.6, 5.3 ± 1.3, and 4.5 ± 0.5%, respectively (Figure S5, Supporting Information). The reduction in loading efficiencies associated with reduced loading volumes may be attributed to an inadequate volume of loading solution to completely wet the 50 mg of pine pollen used for loading. By increasing the volume of loading solution, it was determined that volumes of 1, 2, 3, and 4 mL produced maximum loading efficiencies which were statistically equivalent (p = 0.41 for 1 and 4 mL), with loading efficiencies of 10.6 ± 0.9, 10.1 ± 1.4, 8.5 ± 1.3, and 9.6 ± 1.6%, respectively (Figure S5, Supporting Information).

3.2.3. Loading Distribution Analysis. Loading distribution analysis based upon CLSM imaging of FITC-BSA-loaded NPP, SDPP, and DDPP, indicated that under optimum loading conditions, the majority of pollen particles exhibit some degree of loading, and that loading occurs predominately in air sacs (Figure 5a,b; Figures S6 and S7, Supporting Information). However, air sac loading is typically restricted to the outer portion of the air sac cavity, and the central portion of the air sacs remains empty. On the basis of pollen volumetric measurements above, the outer porous sexine structure comprises ~58% of total air sac volume. Calculations for estimating 100 vol % loading of DDPP indicate that the theoretical maximum potential BSA loading of pine pollen air sacs equates to a BSA loading efficiency of ~18.0%. Therefore, the BSA loading efficiency of 10.6 ± 0.9% obtained with

DOI: 10.1021/acsami.8b09952
ACS Appl. Mater. Interfaces 2018, 10, 28428−28439

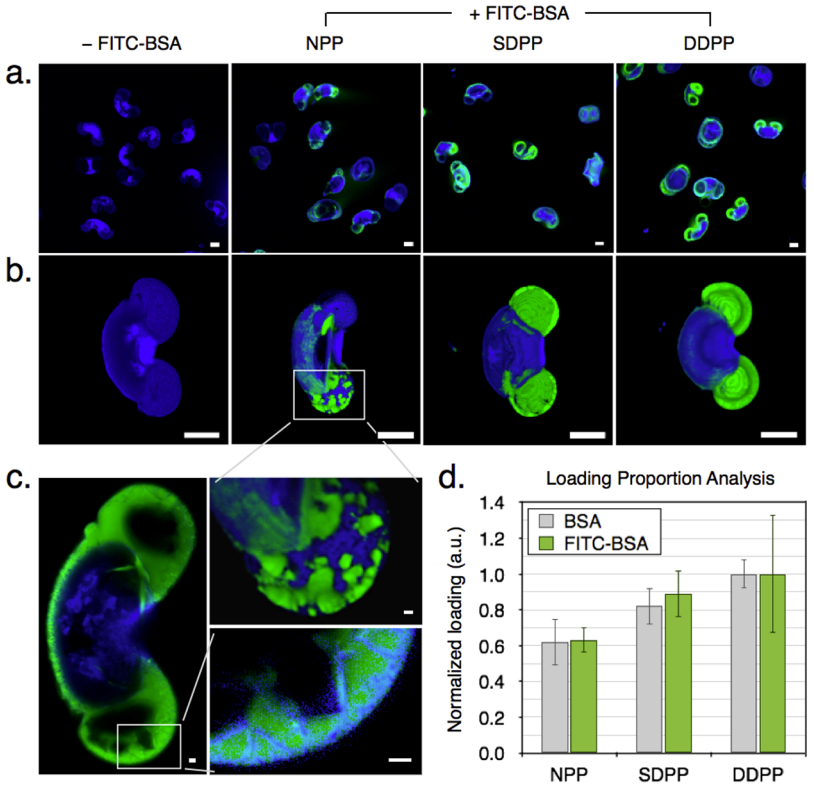

Figure 5. CLSM analysis of vacuum-assisted FITC-BSA-loaded natural and defatted pine pollen: (a) multiparticle images of DDPP without FITC-BSA loading, and NPP, SDPP, and DDPP with FITC-BSA loading; (b) single-particle 3D *z*-stack reconstructions of DDPP without FITC-BSA loading, and NPP, SDPP, and DDPP with FITC-BSA loading; (c) 2D and 3D images of FITC-BSA-loaded NPP and DDPP highlighting FITC-BSA entrapped within the pine pollen porous sexine structure; and (d) comparison of trends between normalized CLSM loading proportion data and conventional loading efficiency data, indicating a high degree of similarity. NPP: natural pine pollen, SDPP: single-defatted pine pollen, DDPP: double-defatted pine pollen. Scale bars: (a,b) = 10 μm; (c) = 2 μm.

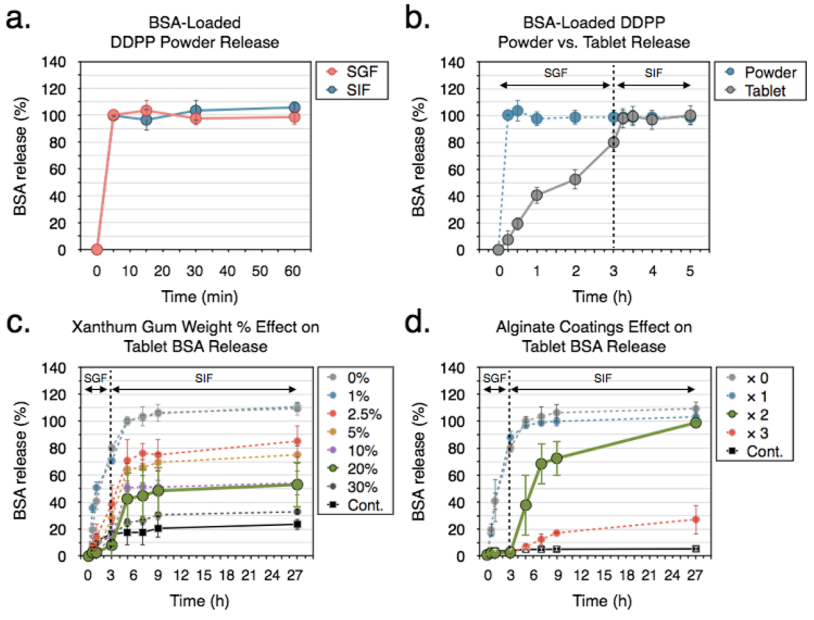

Figure 6. In vitro release profiles of BSA from powdered and tableted BSA-loaded DDPP: (a) BSA release from BSA-loaded DDPP in SGF (pH 1.2) and SIF (pH 7); (b) BSA release from BSA-loaded DDPP powder and tablets with 3 h SGF incubation followed by SIF incubation; (c) xanthan gum weight % effect on BSA release from BSA-loaded DDPP tablets with xanthan gum as a binder, with 3 h SGF incubation followed by SIF incubation; and (d) alginate coating number effect on BSA release from BSA-loaded DDPP tablets coated with ionotropically cross-linked sodium alginate, with 3 h SGF incubation followed by SIF incubation. DDPP: double-defatted pine pollen, SGF: simulated gastric fluid, SIF: simulated intestinal fluid, Cont.: control.

DOI: 10.1021/acsami.8b09952
ACS Appl. Mater. Interfaces 2018, 10, 28428−28439

DDPP highlights that the optimized BSA loading protocols which have been utilized are highly effective.

On the basis of the FITC-BSA loading being restricted to the outer porous sexine structure, as well as the previous observations of water loading of air sacs, it appears that the intricate porous structure of the air sac wall (sexine) tends to trap large molecules, such as BSA (~65 kDa), within the porous shell structure (Figure 5b,c). To support this assertion, the 3D reconstructions of CLSM *z*-stacks depicted in Figure 5b show nonuniform loading of the NPP porous sexine structure, indicating that BSA loading solution may not pass freely between all sexine porous structure cavities. The reason for this effect being highlighted in NPP may be attributed to the presence of lipidic compounds blocking surface nanopores present in the outer exine layer, which may inhibit initial loading of some sexine cavities, whereas when the lipidic compounds are uniformly removed in the SDPP and DDPP, the loading of the porous sexine structure may be more uniform because of the passage of BSA loading solution through sexine surface nanopores, rather than from internal flow between sexine cavities. Additionally, 2D *z*-stack slices of FITC-BSA-loaded DDPP show regions where FITC-BSA is restricted to the micron-sized sexine cavities (Figure 5c).

Loading proportion data from CLSM image analysis and loading efficiency data from loading quantification studies were normalized and compared, with both data sets exhibiting similar trends (Figure 5d). The similarity in loading proportion and loading efficiency trends provides support for the robustness of the loading analysis and suggests that the previous loading optimization studies have been effective. Overall, accurately elucidating compound distribution via CLSM helps to explain the apparently low loading efficiencies observed with natural and defatted pine pollen and provides valuable insight into the potential for further loading optimization.

3.3. Tableted Formulation for Targeted Delivery. Achieving targeted delivery of sensitive compounds, such as proteins, to the intestinal tract typically requires the use of a co-encapsulant to provide adequate gastric protection and allow compound release in a particular environment at a fixed rate.[38,42,44] In this study, only natural co-encapsulants were explored for facilitating the delivery of sensitive proteins to the intestinal tract. BSA-loaded DDPP tablets were prepared with either xanthan gum or alginate. Xanthan gum-based multiparticulate tablets utilized dry xanthan gum powder as a binder in varying proportions, whereas alginate-based multiparticulate tablets utilized ionotropically cross-linked alginate as a coating layer, with varying numbers of coatings.

3.3.1. Compound Release Analysis. Initial release studies were conducted with BSA-loaded DDPP powder before and after tableting. Before tableting, BSA-loaded DDPP powder exhibited a burst release profile, wherein 100% release was observed within 5 min in both SGF and SIF solutions (Figure 6a). After the tableting of BSA-loaded DDPP powder only, some delayed release of BSA was observed. Tablets were exposed to SGF for 3 h, followed by exposure to SIF so as to simulate gastrointestinal tract transit resulting from oral delivery. Three hours in SGF resulted in a release of 80.1 ± 3.0% with the remaining BSA releasing within another 15 min in SIF (Figure 6b). The delayed release observed from the tableting alone may be attributed to the physical robustness of the tablet, with internal BSA-loaded DDPP requiring greater time to become hydrated and release BSA.

The use of xanthan gum as a binder in the tableting of BSA-loaded DDPP powder produced varying degrees of suboptimal controlled release for targeted intestinal delivery depending on the proportion of xanthan gum used. Overall, the addition of xanthan gum in weight fractions of 1, 2.5, 5, 10, 20, and 30 w/w % resulted in the release of 70.6 ± 2.0, 38.5 ± 14.5, 28.3 ± 4.8, 14.1 ± 9.9, 8.1 ± 9.4, and 14.7 ± 2.45% of BSA, respectively, within an initial 3 h in SGF, with an additional release of 27.4 ± 0.6, 46.7 ± 4.7, 46.7 ± 8.7, 40.2 ± 2.8, 44.9 ± 7.7, and 18.1 ± 3.4% of BSA, respectively, with another 24 h in SIF (Figure 6c). Pure xanthan gum and BSA tablets, as a control, exhibited a release of 16.5 ± 9.4% within an initial 3 h in SGF, with an additional release of 7.1 ± 4.2% with another 24 h in SIF, indicating that the inclusion of BSA-loaded DDPP has a meaningful impact on BSA release dynamics. The data indicate that increasing the xanthan gum % not only slows the release of BSA in SGF but also results in incomplete drug release especially with higher xanthan gum fractions. Delayed and incomplete overall BSA release may be attributed to increasing proportions of xanthan gum increasing tablet stability, leading to limited compound diffusion from intact stable tablets. However, the addition of xanthan gum during tableting, in a proportion of 20 w/w %, provides the best suboptimal controlled release profile with only 8.1 ± 9.4% release in SGF for 3 h and an additional 44.9 ± 7.7% release in SIF for another 24 h.

The use of alginate for coating BSA-loaded DDPP powder tablets provided the most ideal release profile for targeted delivery to the intestinal tract. A single coating cycle was achieved by dipping tablets in a 2% aqueous sodium alginate solution, followed by ionotropic cross-linking in a 4% calcium chloride solution. Overall, the addition of ionotropically cross-linked alginate coatings with 1, 2, and 3 coating cycles, resulted in the release of 88.1 ± 4.9, 2.6 ± 0.3, and 2.0 ± 0.0% of BSA, respectively, within an initial 3 h in SGF, with an additional release of 15.8 ± 8.3, 96.0 ± 2.9, and 25.0 ± 10.8% of BSA, respectively, with another 24 h in SIF (Figure 6d). The data indicate that a single coating cycle is inadequate to provide desired release dynamics and that three coating cycles excessively inhibit BSA release in simulated intestinal conditions. However, the application of two coating cycles provides optimal controlled release profile with minimal release in SGF for 3 h (2.6 ± 0.3%) and near complete release in SIF over an additional 24 h (96.0 ± 2.9%). Pure sodium alginate and BSA tablets with dual coating, as a control, exhibited a release of 4.0 ± 1.7% within an initial 3 h in SGF, with an additional release of 1.4 ± 1.5% with another 24 h in SIF, indicating that the inclusion of BSA-loaded DDPP has a beneficial impact on BSA release dynamics. On the basis of these observations, tableting and dual coating of BSA-loaded DDPP may be used to provide an effective all natural formulation for targeted delivery to the intestinal tract.

3.3.2. Tablet Morphology. Tableting of BSA-loaded DDPP powder tablets with varying portions of xanthan gum or coatings of sodium alginate resulted in some variation in tablet morphology. Basic DDPP tablets were prepared with 163.1 ± 0.6 mg of BSA-loaded DDPP, with a diameter of 13.04 ± 0.01 mm and thickness of 1.21 ± 0.01 mm (Table S2, Supporting Information). Xanthan gum-based tablets were prepared by incorporating an additional 1 to 30 wt % of dry xanthan gum, with final tablet weights ranging from 164.2 ± 0.2 to 234.3 ± 0.3 mg, diameters ranging from 13.04 ± 0.01 to 13.10 ± 0.05 mm, and thicknesses ranging from 1.21 ± 0.01 to 1.76 ± 0.01

DOI: 10.1021/acsami.8b09952
ACS Appl. Mater. Interfaces 2018, 10, 28428−28439

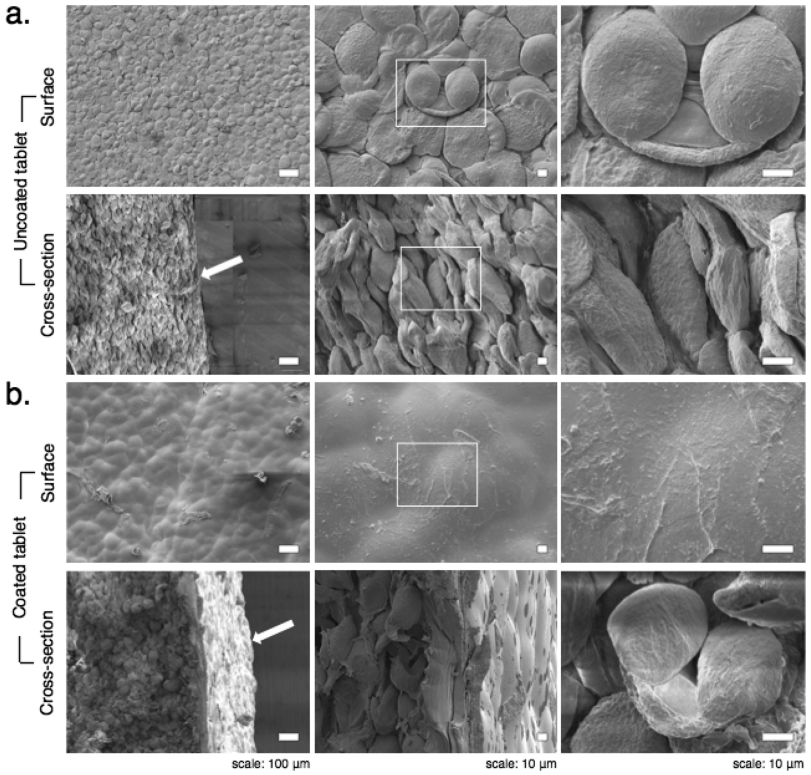

Figure 7. SEM analysis of multiparticulate BSA-loaded defatted pine pollen tablets before and after optimized alginate coating: (a) SEM micrographs of an uncoated multiparticulate BSA-loaded DDPP tablet depicting the tablet surface and cross section, with the white arrow indicating the edge of the tablet cross section; (b) SEM micrographs of an alginate-coated multiparticulate BSA-loaded DDPP tablet depicting the tablet surface and cross section, with the white arrow indicating the surface of the tablet. White boxes indicate areas of magnification. DDPP: double-defatted pine pollen.

mm. Alginate-based tablets were prepared by tableting BSA-loaded DDPP and performing one to three coating cycles with ionotropically cross-linked alginate, with final tablet weights ranging from 168.8 ± 1.9 to 219.0 ± 4.8 mg, diameters ranging from 12.97 ± 0.05 to 12.92 ± 0.03 mm, and thicknesses ranging from 2.27 ± 0.08 to 3.05 ± 0.12 mm. Overall, the weight and thickness of the tablets increased with the % of xanthan gum and number of alginate coatings, whereas the diameter remained nearly constant because of the die press used.

On the basis of two-coat alginate-based tablets providing the most ideal targeted delivery formulation, we proceeded with morphological analysis of tablet surfaces and cross sections, by SEM, before and after alginate coating. Tablets comprising only BSA-loaded DDPP exhibit a rough surface and layered cross-sectional structure because of close packing of compressed discrete pine pollen particles (Figure 7a). Tablets with a coating of ionotropically cross-linked alginate exhibit a smooth surface and a coating layer of ∼30 μm (Figure 7b).

4. CONCLUSIONS

Pine pollen may be utilized as a microencapsulant for compound loading, and completely natural formulations based upon a pine pollen microencapsulation technology can be used for targeted oral delivery applications. The removal of the lipidic compounds adhered to the outer pollen surface improves pollen wetting and exposes nanochannels present in the outer sexine layer, leading to increased water absorption and improved compound loading. Ensuring appropriate vacuum strength, vacuum duration application, loading solution concentration, and washing conditions are required to achieve optimal compound loading. The porous sexine structure is shown to trap large BSA molecules (∼65 kDa), and BSA loading is typically limited to the outer region of the hollow air sac cavity with the central cavity region remaining empty. However, uniform exposure of nanochannels, resulting from defatting, ensures uniform filling of the micron-sized pores of the sexine, allowing for greater overall compound loading.

The development of a multiparticulate tableted formulation, with the application of a natural binder or enteric coating, achieved controlled release properties suited to targeted intestinal delivery of compounds, such as therapeutic proteins. Xanthan gum as a binder provided great ease in tablet preparation, however, exhibited incomplete compound release over a 24 h period. Ionotropically cross-linked alginate coating of defatted pine pollen tablets is a simple multistep process, resulting in ideal release dynamics for intestinal delivery.

Overall, pine pollen exhibits many highly attractive microencapsulant properties and has been shown to provide an effective vehicle for microencapsulation. The large cargo capacity, ease of compound loading, abundant availability, and extensive modern and historical usage of pine pollen make it very appealing for a wide range of practical applications, such as foods, natural cosmetics, traditional herbal therapeutics, or synergistic treatments incorporating modern pharmaceutical compounds, such as therapeutic proteins.

DOI: 10.1021/acsami.8b09952
ACS Appl. Mater. Interfaces 2018, 10, 28428−28439

■ ASSOCIATED CONTENT

Supporting Information

The Supporting Information is available free of charge on the ACS Publications website at DOI: 10.1021/acsami.8b09952.

Scanning electron micrographs of pine pollen cross section; DIPA of natural and defatted pine pollen; optical microscopy images of water filling of natural and defatted pollen; scanning electron micrographs of natural and defatted BSA-loaded pine pollen during washing; loading efficiency quantification for DDPP with varying loading solution volume; CLSM images of FITC-BSA-loaded pine pollen for natural and defatted pollen; CLSM *z*-stack images of unloaded natural pollen and FITC-BSA-loaded pine pollen for natural and defatted pollen; elemental analysis of natural and defatted pine pollen; and details of tableted BSA-loaded DDPP, with and without binder (xanthan gum) or coating (sodium alginate) (PDF)

■ AUTHOR INFORMATION

Corresponding Author

*E-mail: njcho@ntu.edu.sg.

ORCID

Nam-Joon Cho: 0000-0002-8692-8955

Author Contributions

‖A.K.P. and M.G.P. contributed equally.

Notes

The authors declare no competing financial interest.

■ ACKNOWLEDGMENTS

This work was supported by the Competitive Research Programme (NRF-CRP10-2012-07) of the National Research Foundation of Singapore (NRF) and by the Creative Materials Discovery Program through the National Research Foundation of Korea (NRF) funded by the Ministry of Science, ICT, and Future Planning (2016M3D1A1024098). Also, the research was supported by a Start-Up Grant (SUG) from Nanyang Technological University (M4080751.070).

■ REFERENCES

(1) Zhang, Y.; Chan, H. F.; Leong, K. W. Advanced Materials and Processing for Drug Delivery: the Past and the Future. *Adv. Drug Delivery Rev.* **2013**, *65*, 104−120.

(2) Ha, D.; Yang, N.; Nadithe, V. Exosomes as Therapeutic Drug Carriers and Delivery Vehicles Across Biological Membranes: Current Perspectives and Future Challenges. *Acta Pharm. Sin. B* **2016**, *6*, 287−296.

(3) Yoo, J.-W.; Irvine, D. J.; Discher, D. E.; Mitragotri, S. Bio-inspired, Bioengineered and Biomimetic Drug Delivery Carriers. *Nat. Rev. Drug Discovery* **2011**, *10*, 521−535.

(4) Zelikin, A. N.; Ehrhardt, C.; Healy, A. M. Materials and Methods for Delivery of Biological Drugs. *Nat. Chem.* **2016**, *8*, 997−1007.

(5) Atwe, S. U.; Ma, Y.; Gill, H. S. Pollen Grains for Oral Vaccination. *J. Controlled Release* **2014**, *194*, 45−52.

(6) Koziolek, M.; Grimm, M.; Schneider, F.; Jedamzik, P.; Sager, M.; Kühn, J.-P.; Siegmund, W.; Weitschies, W. Navigating the Human Gastrointestinal Tract for Oral Drug Delivery: Uncharted Waters and New Frontiers. *Adv. Drug Delivery Rev.* **2016**, *101*, 75−88.

(7) Wang, H.; Potroz, M. G.; Jackman, J. A.; Khezri, B.; Marić, T.; Cho, N.-J.; Pumera, M. Bioinspired Spiky Micromotors Based on Sporopollenin Exine Capsules. *Adv. Funct. Mater.* **2017**, *27*, 1702338.

(8) Bedinger, P. The Remarkable Biology of Pollen. *Plant Cell* **1992**, *4*, 879−887.

(9) Firon, N.; Nepi, M.; Pacini, E. Water Status and Associated Processes Mark Critical Stages in Pollen Development and Functioning. *Ann. Bot.* **2012**, *109*, 1201−1214.

(10) Blackmore, S.; Knox, R. B. *Microspores Evolution and Ontogeny: Evolution and Ontogeny*; Academic Press, 2016.

(11) Montgomery, W.; Potiszil, C.; Watson, J. S.; Sephton, M. A. Sporopollenin, a Natural Copolymer, is Robust Under High Hydrostatic Pressure. *Macromol. Chem. Phys.* **2016**, *217*, 2494−2500.

(12) Mackenzie, G.; Boa, A. N.; Diego-Taboada, A.; Atkin, S. L.; Sathyapalan, T. Sporopollenin, the Least Known Yet Toughest Natural Biopolymer. *Front. Mater.* **2015**, *2*, 66.

(13) Chiappe, C.; Demontis, G. C.; Di Bussolo, V.; Rodriguez Douton, M. J.; Rossella, F.; Pomelli, C. S.; Sartini, S.; Caporali, S. From Pollen Grains to Functionalized Microcapsules: a Facile Chemical Route Using Ionic Liquids. *Green Chem.* **2017**, *19*, 1028−1033.

(14) Mundargi, R. C.; Potroz, M. G.; Park, J. H.; Seo, J.; Tan, E.-L.; Lee, J. H.; Cho, N.-J. Eco-Friendly Streamlined Process for Sporopollenin Exine Capsule Extraction. *Sci. Rep.* **2016**, *6*, 19960.

(15) Mundargi, R. C.; Potroz, M. G.; Park, J. H.; Seo, J.; Lee, J. H.; Cho, N.-J. Extraction of Sporopollenin Exine Capsules from Sunflower Pollen Grains. *RSC Adv.* **2016**, *6*, 16533−16539.

(16) Potroz, M. G.; Mundargi, R. C.; Park, J. H.; Tan, E.-L.; Cho, N.-j. Extraction of Plant-based Capsules for Microencapsulation Applications. *JoVE* **2016**, *117*, e54768.

(17) Prabhakar, A. K.; Lai, H. Y.; Potroz, M. G.; Corliss, M. K.; Park, J. H.; Mundargi, R. C.; Cho, D.; Bang, S.-I.; Cho, N.-J. Chemical Processing Strategies to Obtain Sporopollenin Exine Capsules from Multi-Compartmental Pine Pollen. *J. Ind. Eng. Chem.* **2017**, *53*, 375−385.

(18) Sargin, I.; Akyuz, L.; Kaya, M.; Tan, G.; Ceter, T.; Yildirim, K.; Ertosun, S.; Aydin, G. H.; Topal, M. Controlled Release and Anti-Proliferative Effect of Imatinib Mesylate Loaded Sporopollenin Microcapsules Extracted from Pollens of Betula Pendula. *Int. J. Biol. Macromol.* **2017**, *105*, 749−756.

(19) Barrier, S.; Rigby, A. S.; Diego-Taboada, A.; Thomasson, M. J.; Mackenzie, G.; Atkin, S. L. Sporopollenin Exines: A Novel Natural Taste Masking Material. *LWT–Food Sci. Technol.* **2010**, *43*, 73−76.

(20) Diego-Taboada, A.; Beckett, S.; Atkin, S.; Mackenzie, G. Hollow Pollen Shells to Enhance Drug Delivery. *Pharmaceutics* **2014**, *6*, 80−96.

(21) Atkin, S. L.; Barrier, S.; Cui, Z.; Fletcher, P. D. I.; Mackenzie, G.; Panel, V.; Sol, V.; Zhang, X. UV and Visible Light Screening by Individual Sporopollenin Exines Derived from Lycopodium Clavatum (club moss) and Ambrosia Trifida (giant ragweed). *J. Photochem. Photobiol., B* **2011**, *102*, 209−217.

(22) Uddin, M. J.; Gill, H. S. Ragweed Pollen as an Oral Vaccine Delivery System: Mechanistic Insights. *J. Controlled Release* **2017**, *268*, 416−426.

(23) Wakil, A.; Mackenzie, G.; Diego-Taboada, A.; Bell, J. G.; Atkin, S. L. Enhanced Bioavailability of Eicosapentaenoic Acid from Fish Oil After Encapsulation Within Plant Spore Exines as Microcapsules. *Lipids* **2010**, *45*, 645−649.

(24) Feás, X.; Vázquez-Tato, M. P.; Estevinho, L.; Seijas, J. A.; Iglesias, A. Organic Bee Pollen: Botanical Origin, Nutritional Value, Bioactive Compounds, Antioxidant Activity and Microbiological Quality. *Molecules* **2012**, *17*, 8359−8377.

(25) Llnskens, H. F.; Jorde, W. Pollen as food and medicine-A review. *Econ. Bot.* **1997**, *51*, 78−86.

(26) Waldbott, G. L. Pollen in Medicine. *Rev. Palaeobot. Palynol.* **1967**, *4*, 247−249.

(27) Larkin, T. *Bee Pollen as a Health Food*; FDA Consumer, 1984.

(28) Almeida-Muradian, L. B.; Pamplona, L. C.; Coimbra, S.; Barth, O. M. Chemical Composition and Botanical Evaluation of Dried Bee Pollen Pellets. *J. Food Compos. Anal.* **2005**, *18*, 105−111.

(29) Punt, W.; Hoen, P. P.; Blackmore, S.; Nilsson, S.; Le Thomas, A. Glossary of Pollen and Spore Terminology. *Rev. Palaeobot. Palynol.* **2007**, *143*, 1−81.

DOI: 10.1021/acsami.8b09952
ACS Appl. Mater. Interfaces 2018, 10, 28428−28439

(30) Li, Q.; Gluch, J.; Krüger, P.; Gall, M.; Neinhuis, C.; Zschech, E. Pollen Structure Visualization Using High-Resolution Laboratory-based Hard X-ray Tomography. *Biochem. Biophys. Res. Commun.* **2016**, *479*, 272−276.
(31) Schwendemann, A. B.; Wang, G.; Mertz, M. L.; McWilliams, R. T.; Thatcher, S. L.; Osborn, J. M. Aerodynamics of Saccate Pollen and its Implications for Wind Pollination. *Am. J. Bot.* **2007**, *94*, 1371−1381.
(32) Bohne, G.; Richter, E.; Woehlecke, H.; Ehwald, R. Diffusion Barriers of Tripartite Sporopollenin Microcapsules Prepared from Pine Pollen. *Ann. Bot.* **2003**, *92*, 289−297.
(33) Bohne, G.; Woehlecke, H.; Ehwald, R. Water Relations of the Pine Exine. *Ann. Bot.* **2005**, *96*, 201−208.
(34) Pacini, E.; Franchi, G. G.; Ripaccioli, M. Ripe Pollen Structure and Histochemistry of Some Gymnosperms. *Plant Syst. Evol.* **1999**, *217*, 81−99.
(35) Hess, W. M.; Weber, D. J.; Allen, J. V.; Laseter, J. L. Ultrastructural Changes Caused by Lipid Extraction of Pollen of Pinus Echinata. *Can. J. Bot.* **1973**, *51*, 1685−1688.
(36) Tomlinson, P. Structural Features of Saccate Pollen Types in Relation to their Functions. *Pollen and Spores: Morphology and Biology*; Royal Botanic Gardens, 2000; pp 147−162.
(37) Grega, L.; Anderson, S.; Cheetham, M.; Clemente, M.; Colletti, A.; Moy, W.; Talarico, D.; Thatcher, S. L.; Osborn, J. M. Aerodynamic Characteristics of Saccate Pollen Grains. *Int. J. Plant Sci.* **2013**, *174*, 499−510.
(38) Potroz, M. G.; Mundargi, R. C.; Gillissen, J. J.; Tan, E.-L.; Meker, S.; Park, J. H.; Jung, H.; Park, S.; Cho, D.; Bang, S.-I.; Cho, N.-J. Plant-Based Hollow Microcapsules for Oral Delivery Applications: Toward Optimized Loading and Controlled Release. *Adv. Funct. Mater.* **2017**, *27*, 1700270.
(39) Cho, A. J. *Investigation into the Amination and Thiolation of Sporopollenin*; The University of Hull, 2003.
(40) Sing, K. S. W. Reporting Physisorption Data for Gas/Solid Systems with Special Reference to the Determination of Surface Area and Porosity (Recommendations 1984). *Pure Appl. Chem.* **1985**, *57*, 603−619.
(41) Wittborn, J.; Rao, K. V.; El-Ghazaly, G.; Rowley, J. R. Nanoscale Similarities in the Substructure of the Exines ofFagusPollen Grains andLycopodiumSpores. *Ann. Bot.* **1998**, *82*, 141−145.
(42) Mundargi, R. C.; Potroz, M. G.; Park, S.; Park, J. H.; Shirahama, H.; Lee, J. H.; Seo, J.; Cho, N.-J. LycopodiumSpores: A Naturally Manufactured, Superrobust Biomaterial for Drug Delivery. *Adv. Funct. Mater.* **2016**, *26*, 487−497.
(43) Mundargi, R. C.; Potroz, M. G.; Park, S.; Shirahama, H.; Lee, J. H.; Seo, J.; Cho, N.-J. Natural Sunflower Pollen as a Drug Delivery Vehicle. *Small* **2016**, *12*, 1167−1173.
(44) Talley, K.; Alexov, E. On the pH-Optimum of Activity and Stability of Proteins. *Proteins* **2010**, *78*, 2699−2706.

DOI: 10.1021/acsami.8b09952
ACS Appl. Mater. Interfaces 2018, 10, 28428−28439